Joule

CellPress

Article

Utilization of Trapped Optical Modes for White Perovskite Light-Emitting Diodes with Efficiency over 12%

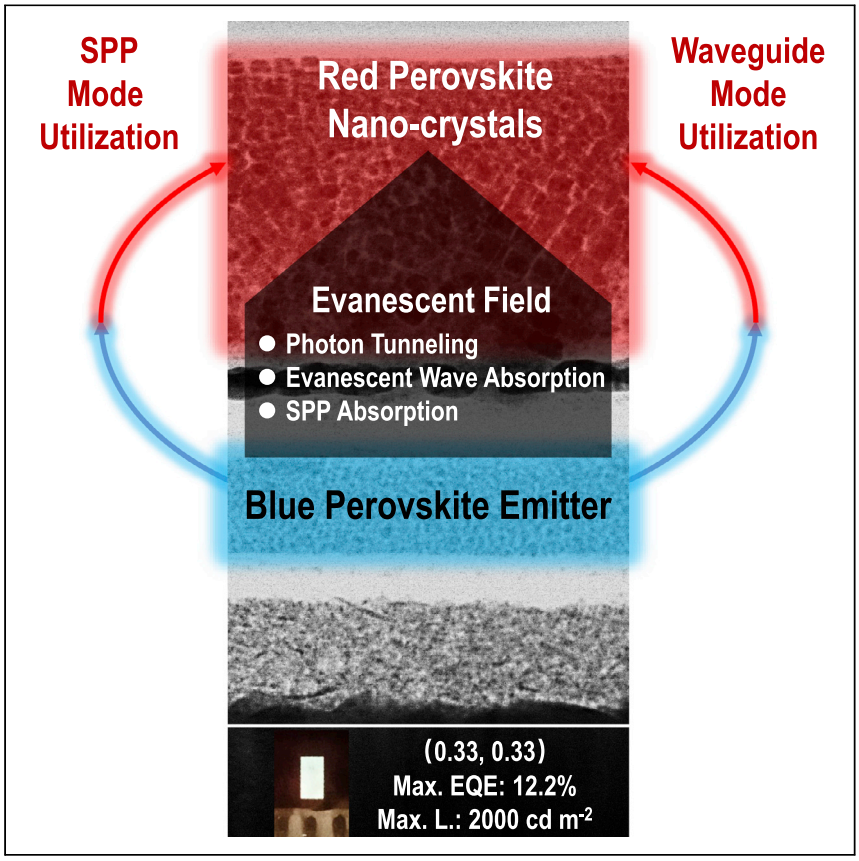

Through the utilization of near-field coupling between different emitters via evanescent fields, we rationally design a novel device structure for efficient white perovskite light-emitting diodes (LEDs), in which a red perovskite nanocrystal layer successfully extracts the trapped blue photons and converts them to emissive red photons. Besides perovskite LEDs, such a mechanism should be feasible for other LED chip designs, such as inorganic, quantum dot, and hybrid LEDs, etc., which might address the issues currently facing in commercial white LEDs.

Ziming Chen, Zhenchao Li, Zhen Chen, ..., Junbiao Peng, Hin-Lap Yip, Yong Cao

chenziming@scut.edu.cn (Z.C.)
msangusyip@scut.edu.cn (H.-L.Y.)

HIGHLIGHTS

The best 2- and 3-color white PeLEDs with >12% and >5% efficiencies, respectively

A rational device design that utilizes near-field optics to extract trapped photons

Waveguide mode can be extracted by photon tunneling and evanescent wave absorption

Surface plasmon polariton mode can be utilized by reabsorption/reemission process

Chen et al., Joule 5, 456–466
February 17, 2021
https://doi.org/10.1016/j.joule.2020.12.008

CellPress

Joule

Article

Utilization of Trapped Optical Modes for White Perovskite Light-Emitting Diodes with Efficiency over 12%

Ziming Chen,[1,2,6,*] Zhenchao Li,[1,6] Zhen Chen,[1] Ruoxi Xia,[1] Guangruixing Zou,[1] Linghao Chu,[1] Shi-Jian Su,[1] Junbiao Peng,[1] Hin-Lap Yip,[1,3,4,5,7,*] and Yong Cao[1]

SUMMARY

The inferior light extraction efficiency (LEE), which is generally less than 20%, based on optical modeling, and the difficulty in achieving white emission are the two main challenges in the metal-halide-perovskite light-emitting diode (PeLED) field. Herein, we report a simple and efficient approach to construct high-performance white PeLEDs with much-enhanced LEE by coupling a blue PeLED with a layer of red perovskite nanocrystal (PeNC) down-converter through a rationally designed multilayer semitransparent electrode (LiF/Al/Ag/LiF). The red PeNC layer allows the extraction of the trapped waveguide mode and surface plasmon polariton mode in a blue PeLED and converts them to red emission, resulting in over 50% LEE improvement. Simultaneously, the complementary emission spectrum of blue photons and down-converting red photons contributes to a white PeLED with a high external quantum efficiency and luminance of more than 12% and approximately 2,000 cd m^{-2}, respectively, which represent state-of-the-art results in this field.

INTRODUCTION

White light-emitting diodes (LEDs) are the important components in lighting and display applications, which consume a large portion of energy in our daily life; therefore, an efficient white LED is important for energy saving and carbon footprint reduction. Metal-halide perovskite LEDs (PeLEDs) show great potential to be the next-generation lighting technology, with external quantum efficiencies (EQEs) improved from less than 1% to more than 20% for red and green LEDs and more than 12% for blue LEDs.[1–13] However, with efficiencies approaching the theoretical limits, the inferior light extraction efficiency (LEE) of PeLEDs, which is generally less than 20%, based on optical modeling, becomes one of the main issues limiting their further development.[14,15] In addition, the integration of different-colored PeLEDs for a white PeLED (WPeLED) is another great challenge in this field. So far, the best all-perovskite white LEDs based on a tandem structure and a rare-earth-ion-doped perovskite only show inferior EQEs of ~0.2% and ~1.2%, respectively.[16,17] Therefore, the development of new strategies to improve the LEE of PeLEDs while fulfilling white-light emission is urgently needed, and it will be of great merit if both challenges can be addressed simultaneously.

In PeLEDs, the generated light in the emissive layer induces a series of optical modes within the device, including waveguide mode, surface plasmon polariton (SPP) mode, substrate mode, and out-coupled mode. Generally, only out-coupled

Context & Scale

Substantial developments of red, green, and blue perovskite light-emitting diodes (PeLEDs) have been achieved; however, a great lag still exists in the development of white PeLEDs. In addition, in a conventional PeLED, based on optical modeling, over 80% of photons are generally trapped within the device. Here, we rationally design a PeLED structure that simultaneously achieves white emission and extracts trapped photons for better performance. In our white PeLED, a red perovskite nanocrystal (PeNC) layer is deposited above the thin electrode of semitransparent blue PeLED, which allows a near-field coupling between red and blue perovskite emitters. The red PeNC layer extracts the trapped photons from the blue PeLED and down-converts them to red photons, resulting in a white PeLED with high efficiency of over 12%. Our PeLED design provides an alternative nanoscale light out-coupling strategy to improve device performance and paves the way for the development of efficient white PeLEDs.

mode (< 20%) contributes to the LEE while SPP mode (20%–30%), waveguide mode (20%–30%), substrate mode (10%–30%), and parasitic absorption (<10%) are consumed within the device.[6,14,15] In commercial LEDs, substrate mode is efficiently suppressed by forming an epoxy optical lens on the substrate side during encapsulation, and for white emission, fluorescent powders are generally dispersed in the epoxy lens to convert photons from the blue chip. Other strategies, such as forming functional array or grating by photolithography, are also developed to improve the extraction of waveguide and SPP modes. However, these well-developed methods may not necessarily be suitable for PeLEDs due to different device structures and fabrication processes. Therefore, new approaches, such as the introduction of surface texturing, photonic crystals, and perovskite nanophotonic wire arrays, have been developed to improve the waveguide mode extraction of PeLEDs.[18–20] Nevertheless, it is still critical to develop a much simpler and cost-effective method to efficiently extract both waveguide and SPP modes simultaneously to further improve the LEE and performance of PeLEDs.

RESULTS AND DISCUSSION

Waveguide and SPP Modes in PeLEDs

Waveguide mode is generated in functional layers of PeLED due to the total internal reflection (TIR) induced by the large difference in the refractive indices (n) between the perovskite layers (large n) and organic charge-transport layers (small n). In a typical PeLED with inverted structure, as illustrated in Figure 1A, when photons generated in perovskite layer propagate to the 1,3,5-tris(1-phenyl-1H-benzimidazol-2-yl)benzene (TPBi)/metal-cathode interface (with any incident angle) and perovskite/TPBi interface (with incident angle larger than the critical angle), TIR occurs and evanescent wave 1 and evanescent wave 2 are generated, respectively. Although no actual photon can propagate to the next layer, the energy of the evanescent wave still penetrates into the upper film and its intensity exponentially dissipates in the z direction in nanometer scale for visible light, suggesting its near-field property. More importantly, as illustrated in Figure 1A, evanescent waves 1 and 2 can further excite the SPPs (Kretschmann type at the air/metal-electrode interface and Otto type at the TPBi/metal-electrode interface, respectively) via matching of the wave vectors in the x direction of evanescent waves (k_{x1} and k_{x2}) and wave vectors of SPPs (k_{SPP1} and k_{SPP2}), i.e., $k_{x1} = k_{SPP1}$ and $k_{x2} = k_{SPP2}$, respectively (detailed discussion can be found in Supplemental Experimental Procedures and Figures S1–S3).[21] The two types of SPPs propagate along the metal-electrode surface and are absorbed by the metal electrode finally, causing a 20%–30% loss of light in PeLED. Note that in the z direction, the SPP is also an evanescent field that decays exponentially in both metal (generally <20 nm) and dielectric sides (generally >100 nm).[22] Because both the evanescent fields produced by TIR and SPP penetrate to the adjacent layers in the near field, this provides us with an opportunity to wisely utilize them to suppress the waveguide and SPP modes in PeLEDs.

Rational PeLED Design and Its Working Mechanism

To simultaneously utilize the waveguide and SPP modes, we designed a PeLED architecture consisting of indium tin oxide (ITO)/NiO_x/poly(9-vinylcarbazole) (PVK)/sky-blue perovskite/TPBi/LiF/Al/Ag/LiF/red perovskite nanocrystals (PeNCs), as shown in Figures 1B and S4; its energy-level diagram is shown in Figure S5. Detailed characterizations of sky-blue perovskite (with 493-nm emission) can be found in Figure S6. LiF/Al/Ag/LiF is a semitransparent electrode with 86% transparency at 493 nm (Figure S7), which allows the energy penetration of sky-blue photons to the compact 650-nm red-emissive $CsPbBrI_2$ PeNC layer (Figure S8). Here, LiF/Al/Ag serves as an efficient cathode where LiF/Al reduces the work function and Ag

[1]State Key Laboratory of Luminescent Materials and Devices, School of Materials Science and Engineering, South China University of Technology, 381 Wushan Road, Guangzhou 510640, P.R. China

[2]School of Environment and Energy, South China University of Technology, Guangzhou University City, Panyu District, Guangzhou 510006, P.R. China

[3]Innovation Center of Printed Photovoltaics, South China Institute of Collaborative Innovation, Dongguan 523808, P.R. China

[4]Department of Materials Science and Engineering, City University of Hong Kong, Tat Chee Avenue, Kowloon, Hong Kong

[5]School of Energy and Environment, City University of Hong Kong, Tat Chee Avenue, Kowloon, Hong Kong

[6]These authors contributed equally

[7]Lead Contact

*Correspondence: chenziming@scut.edu.cn (Z.C.), msangusyip@scut.edu.cn (H.-L.Y.)

https://doi.org/10.1016/j.joule.2020.12.008

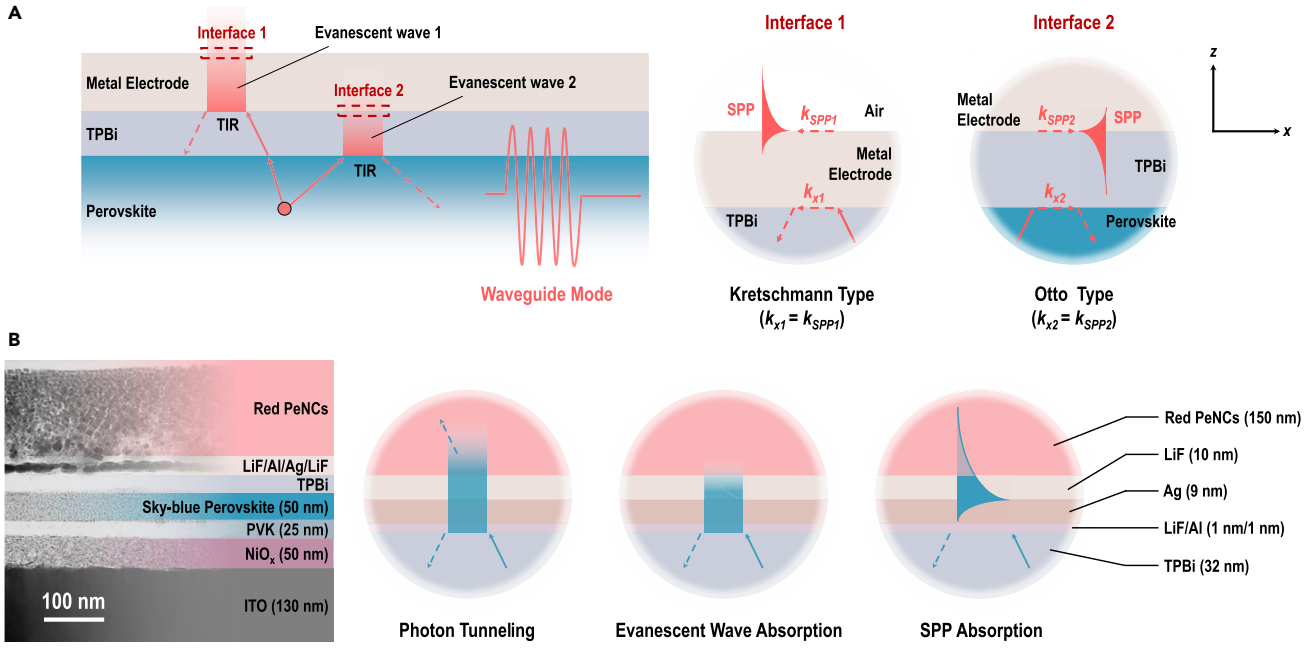

Figure 1. Waveguide Mode, SPP Mode, and Their Utilizations in PeLEDs

(A) Schematic diagram of two types of SPPs (Kretschmann and Otto types) induced by evanescent waves 1 and 2, respectively. k_{x1} and k_{x2} represent wave vectors of evanescent waves in the *x* direction at the TPBi/metal-electrode and TPBi/perovskite interfaces, respectively, while k_{SPP1} and k_{SPP2} represent the wave vectors of SPPs at air/metal-electrode and TPBi/metal-electrode interfaces, respectively.

(B) Cross-section scanning transmission electron microscope (STEM) image of the best WPeLED developed herein and a schematic diagram showing the three different optical effects presented in the metal electrode side of the WPeLED. Each layer in the device is identified by the energy dispersive spectroscopy shown in Figure S4.

provides a high conductivity for the electrode,[23] while the upper LiF layer, which is above the Ag film, serves as a blocking layer that suppresses the PL quenching between red PeNC and Ag interface.

This device structure allows us to utilize the waveguide and SPP modes in PeLED via three special effects, including photon tunneling, evanescent wave absorption, and SPP absorption, as illustrated in Figure 1B. Photon tunneling is the effect that allows photons in TIR condition to still tunnel to another material via overwhelming the optical barrier, which occurs when a large-*n* material exists within the penetration depth of the evanescent wave.[24] According to Figure S9, the penetration depth of evanescent wave 1 is confirmed to be around 290 nm; therefore, under TIR condition, the sky-blue photons in the relatively large-*n* TPBi layer (n = 1.75, *n* value of each layer can be found in Figure S3A) can still overwhelm the optical barrier from the 21-nm LiF/Al/Ag/LiF multiple layers (with small *n* of 1.37/0.74/0.02/1.37, respectively) and then tunnel to the large-*n* red PeNC layer (n = 2.1). A similar photon tunneling process from sky-blue perovskite to the red PeNC layer can also occur for evanescent wave 2, with a penetration depth reaching 300 nm (Figure S9). Through photon tunneling, the extraction of sky-blue photons dramatically improves and becomes approximately 2.5-times larger than that without the red PeNC layer (detailed discussion can be found in Supplemental Experimental Procedures and Figures S10 and S12). Besides, the energy of sky-blue evanescent waves penetrated to the red PeNC layer can also be absorbed due to the large extinction coefficients of red PeNCs for sky-blue photons (Figure S3B), which further results in a down-converting emission of red photons. Both the above

effects consume sky-blue photons in TIR condition and therefore efficiently suppress the waveguide mode within the device.

Moreover, similar to the evanescent wave-absorption effect, the Kretschmann-type SPP generated at the Ag/LiF interface can be absorbed by the red PeNC layer (Figure 1B), because of its decent penetration depth of 196 nm on the LiF side (Figure S12), which also converts the SPP to red emissive photons and hence suppresses the SPP mode in the PeLED. However, this system cannot utilize the Otto-type SPP generated at the TPBi/metal electrode interface due to the rapid drop of intensity in the *z* direction toward the PeNC layer. This SPP would possibly recouple with the waveguide mode because of its penetration depth on the TPBi side, reaching 73 nm (Figure S12). Consequently, our device design provides three channels for the trapped photons to escape from the emissive layer and hence suppress the waveguide and SPP modes simultaneously, which benefits the device performance.

Device Performances of WPeLEDs

The overall device properties are shown in Figure 2. As both the cathode and anode of the device are transparent, our sky-blue PeLED (without red PeNCs layer) and WPeLED (with red PeNCs layer) can emit light on both sides of the device, as shown in Videos S1 and S2, respectively. The measurement system for recording the device properties is illustrated in Figure S13. For sky-blue PeLED, the thickness of each layer, as shown in Figure 1B, has been fully optimized to acquire the best device performance, noting that the Ag electrode is reduced to a minimum thickness of 9 nm to obtain high transparency, while still possessing good mechanical and electrical properties for normal device operation (Figure S14). Accordingly, for the investigation of WPeLED, all the layer thicknesses are the same as the optimized sky-blue PeLED except the upper LiF thickness is further finely tuned and the introduction of the red PeNC layer. Figure 2A shows that the average EQE of the WPeLED (~10.4%) is more than 50% greater than that of its sky-blue counterpart (~6.9%). Figures 2B and 2C demonstrate that the best WPeLED obtains the highest EQE of 12.2%, which is 60 times greater than the best reported EQE of a two-color WPeLED (~0.2%) to date.[16] The current efficiency and power efficiency of this device are shown in Figures S15A and S15B, respectively. And the calculated EQE of the sky-blue part in WPeLED (Figure S15C) is smaller than that of the pristine sky-blue device, which suggests that the existence of red PeNC layer in WPeLED cannot enhance the EQE of the bottom sky-blue cell. Instead, the EQE improvement should result from the successful extraction of trapped sky-blue photons by the red PeNC layer. Moreover, the overlapped current density-voltage (*J-V*) curves of the sky-blue PeLED and WPeLED further support the idea that the extra layer of red PeNCs does not affect the electrical property of the WPeLED. Therefore, we can attribute its improved efficiency purely to the optical gain from our device design (i.e. over 50% LEE improvement).

Figures 2D and 2E show that the EL spectrum of WPeLED is composed of two complementary colors, sky blue (493 nm) and red (650 nm), which contribute to pure white light with Commission Internationale de l'Eclairage (CIE) coordinates of (0.33, 0.33). Moreover, the WPeLED under various applied voltages or a constant current (Figure S16) obtains excellent spectral stability, with no shift of the spectrum or CIE coordinates. It is noteworthy that the emission from each side of the device is different because of their different out-coupling profiles. Nevertheless, the emission from both sides still possesses a Lambertian distribution and the emission spectra are stable in all the emission angles, which suggests that no obvious optical cavity

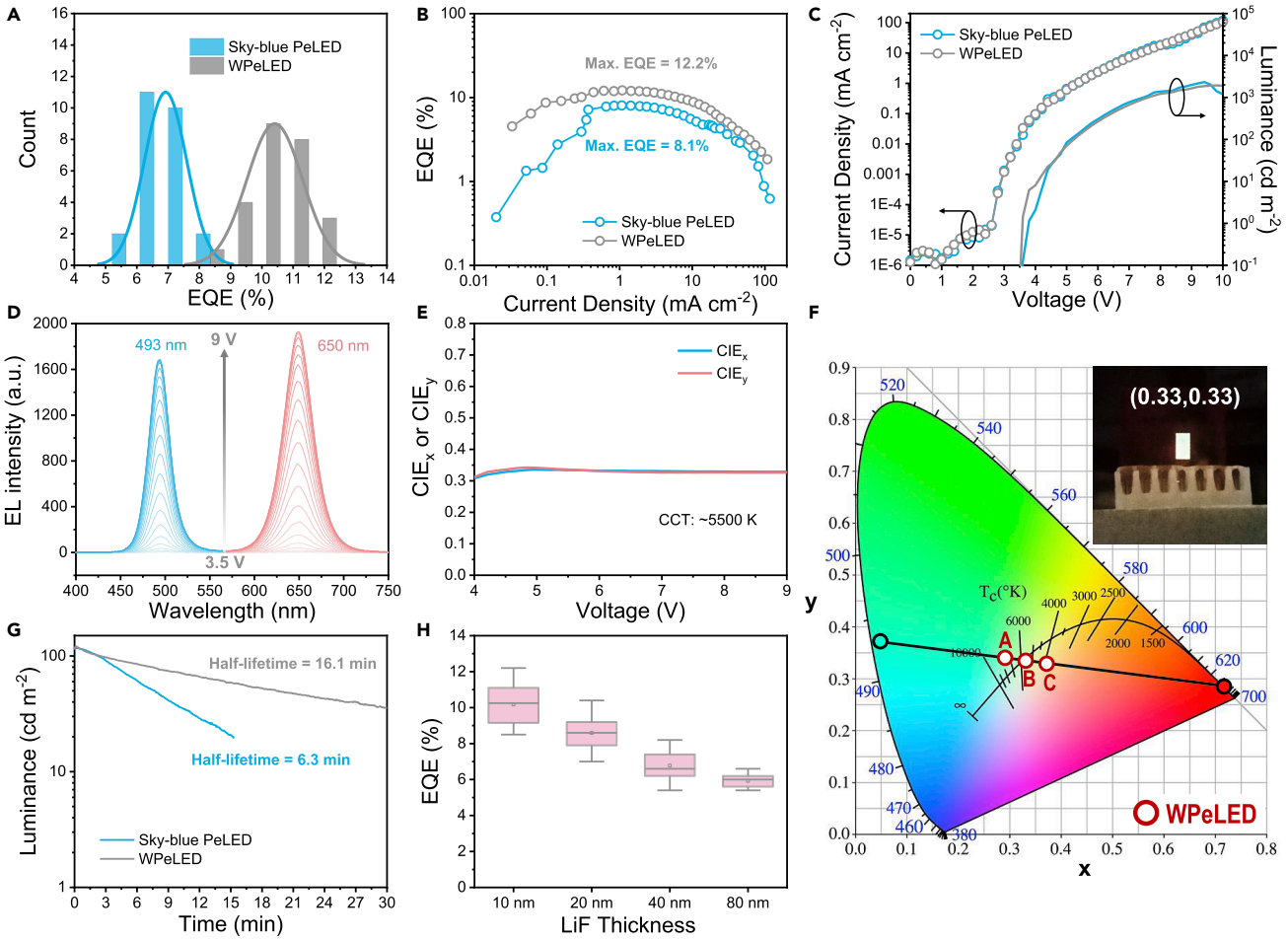

Figure 2. Device Properties of Sky-blue PeLEDs and WPeLEDs

(A) Statistical EQEs of 25 sky-blue PeLEDs and WPeLEDs, respectively.

(B) Current density–EQE curves of the best WPeLED and its sky-blue counterpart.

(C) *J–V* curves and luminance–voltage curves of the best WPeLED and its sky-blue counterpart.

(D) EL spectra and (E) x (CIE_x) and y (CIE_y) values in CIE coordinates of WPeLED under various applied voltages.

(F) CIE coordinates of WPeLEDs and Points A (0.29, 0.34), B (0.33, 0.33) and C (0.37, 0.32) represent 3 devices with various thicknesses of red PeNC layer. The inset is a photo of a WPeLED (Point B).

(G) Device lifetimes of a WPeLED and its sky-blue counterpart.

(H) The relationship between the statistical EQEs of 15 WPeLEDs and the thickness of the upper LiF layer.

effect exists in our device and that all the perovskite emitters are isotropic (Figure S17). Besides, Figures 2F and S18 show that the correlated color temperature (CCT) of white light could be easily tuned from approximately 7,500 to 3,750 K by modulating the thickness of red PeNC layer (from Points A to C). Interestingly, as shown in Figure 2G, the WPeLED has a much longer device half-lifetime (16.1 min) than its sky-blue counterpart (6.3 min), which we attribute to the release of trapped photons suppressing the local heat in the perovskite emitter, which is considered as a key degradation mechanism for PeLED.[23] Moreover, to examine the near-field working mechanism, we gradually increase the thickness of the upper LiF layer from 10 nm to 80 nm. Figure 2H shows that the EQEs decrease with increasing LiF thickness, which proves again that the evanescent field coupling is a near-field effect and is very sensitive to the coupling distance. With a smaller distance between the evanescent fields and red PeNCs, a better device efficiency is achieved. Note that further decreasing the thickness of the upper LiF layer (e.g., 5 nm) results in a failure

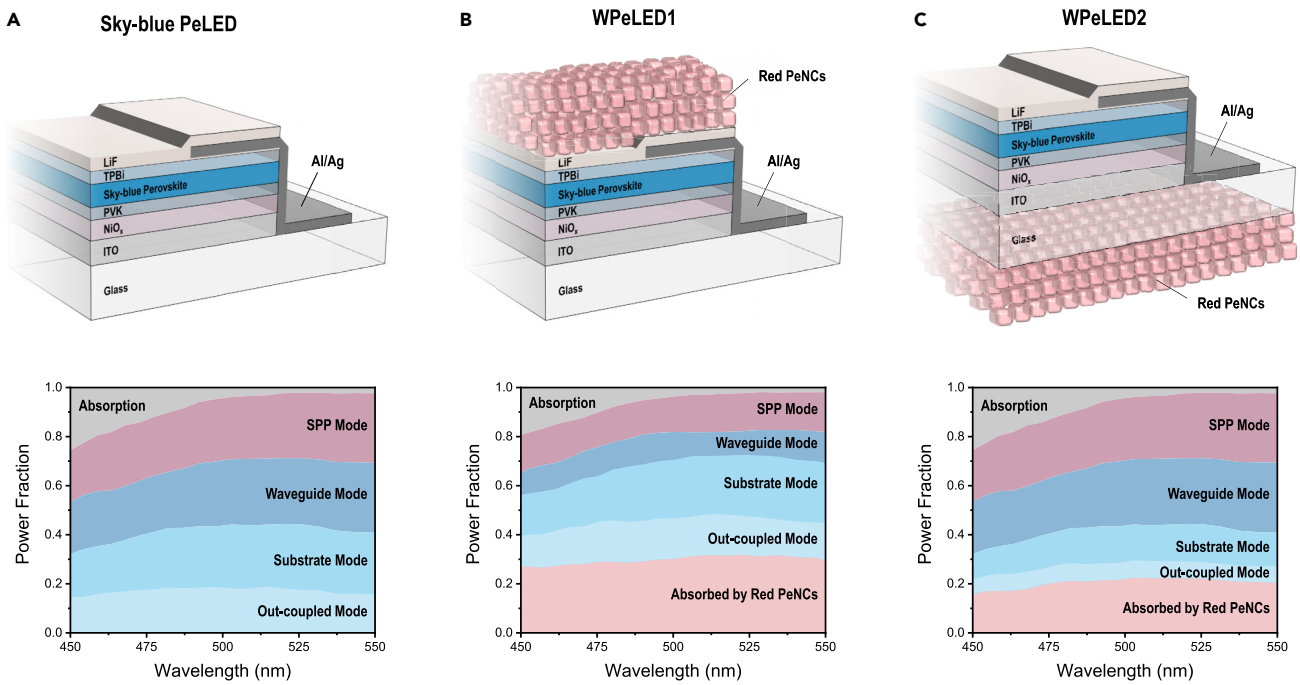

Figure 3. Device Architectures of PeLEDs and Power Fractions of Different Optical Modes in PeLEDs

(A) Sky-blue PeLEDs.

(B) WPeLED1.

(C) WPeLED2.

of the device, which probably due to the damage of the device when processing the upper red PeNC layer as the thin LiF layer cannot provide sufficient protection to the underneath layers.

Optical Analysis of PeLEDs

To further investigate the differences among the sky-blue PeLED, our WPeLED (marked as WPeLED1), and the WPeLED with conventional white LED structure that deposits fluorescent powder (red PeNCs) on the substrate side (marked as WPeLED2), we conducted a finite-difference time-domain (FDTD) simulation to provide a deeper understanding of the optical-mode distribution within the device. Figure 3A shows that in sky-blue PeLED, at 493 nm, around 24.6%, 26.1%, 25.1%, and 5.7% photons are consumed for the substrate mode, waveguide mode, SPP mode, and parasitic absorption, respectively, resulting in a low LEE of around 18.5%. However, in WPeLED1 at 493 nm, 29.5% of the blue photons are absorbed by the red PeNC layer through the channels of SPP absorption (11.2%), photon tunneling (7.0%), evanescent wave absorption (6.6%), and other optical modes (4.7%) (Figure S19), resulting in a reduction of total power fraction of the waveguide and SPP modes from 51.2% of the original device to 25.9% in the WPeLED1. While in WPeLED2, around 21.4% photons are absorbed by the red PeNC layer, resulting in a considerable consumption of out-coupled photons (11.6%) despite the decent suppression of substrate mode (9.8%). After photon absorption, the red PeNC layer can emit red photons with a PLQY of 40% (Figures S8C and S8D); therefore, according to Table 1 and WPeLED2 performance shown in Figure S20, the calculated optical gain for WPeLED1 and WPeLED2 are +54.1% and −13.5%, respectively, showing a consistency with the experimental EQE changes of +50.7% and −15.9%.

Table 1. LEEs and Optical Gains from FDTD Simulations at 493 nm and Experimental Results

	LEE for Sky-Blue Photons	Light Extraction by Red PeNCs Layer[a]	Total LEE	Calculated Optical Gain[b]	Experimental EQE[c]	Experimental EQE Change[d]
Sky-Blue PeLED	18.5%	–	18.5%	–	6.9%	–
WPeLED1	16.7%	11.8% (29.5% × 40%)	28.5%	+54.1%	10.4%	+50.7%
WPeLED2	7.4%	8.6% (21.4% × 40%)	16.0%	−13.5%	5.8%	−15.9%

[a]This value equals the portion of sky-blue photons absorbed by the red PeNC layer (29.5% for WPeLED1 and 21.4% for WPeLED2) times the PLQY value of the red PeNC thin film (40%)

[b][Total LEE (WPeLED1 or WPeLED2) − Total LEE (sky-blue PeLED)]/Total LEE (sky-blue PeLED)

[c]These are the average EQE values of 25 devices

[d][Experimental EQE (WPeLED1 and WPeLED2) − Experimental EQE (sky-blue PeLED)]/Experimental EQE (sky-blue PeLED)

Moreover, the extraction speeds of sky-blue photons in WPeLED1 and WPeLED2 are also evaluated by FDTD. For WPeLED1, Figure S21A and Video S3 show that photons generated in the sky-blue perovskite layer are easily trapped within the device at an early stage, but these trapped photons rapidly dissipate (within 100 fs) by tunneling to and being absorbed by the red PeNCs layer. Such a sky-blue photon-extraction process in the device rapidly dissipates the waveguide mode and hence should suppress the photon-recycling process, which also contributes to a higher LEE in PeLED.[25] Meanwhile, in WPeLED2, Figure S21B and Video S4 show that the sky-blue photons are trapped within the device for a long period of time, which might result in a relatively obvious photon recycling effect in the device.

Consequently, the overall LEE is dramatically improved in WPeLED1, resulting from the rapid utilization of dominantly trapped optical modes (waveguide and SPP modes) with a slight consumption of out-coupled photons, while the WPeLED2 shows a much lower overall LEE for the considerable consumption of out-coupled photons. This problem is also found in commercial white LEDs that comprise an InGaN/GaN blue-chip and far-field YAG yellow fluorescent powder.

Conclusions

We have developed a simple device structure for efficient WPeLEDs by utilizing evanescent fields generated in TIR and SPP conditions. The near-field effects of photon tunneling, evanescent wave absorption, and SPP absorption are exploited to extract the trapped blue photons in the waveguide and SPP modes to the red perovskite fluorescent layer and then convert them to red photons. Furthermore, this nanoscale-control of the evanescent field also provides LEE and EQE improvements of more than 50% from blue to white devices and also enhances device stability. The high EQE of 12.2% and high luminance of 2,000 cd m^{-2} both represent the most efficient WPeLED to date, establishing a milestone in the WPeLED field.

Notably, the PLQY of our red perovskite fluorescent layer is relatively low (40%) and the substrate mode is still trapped within the device (~25%); a much higher WPeLED efficiency can be expected if a higher-PLQY perovskite fluorescent powder and a general epoxy optical lens for substrate mode extraction can be used. Besides, considering the low color rendering index (CRI) of this two-color white light (−66), it is not suitable for the application of white-light illumination; however, it should be competent for the potential applications that only need to recognize the white light source by eye or camera, such as lighting signs, advertising boards, and art creations, as well as light painting. To prove that our device design is also compatible with other applications that require multicolor white light, we demonstrate a three-color all-perovskite white LED with 5.2% EQE and 69 CRI by changing the sky-blue

perovskite emitter to a pure-blue one and adding a yellowish-green PeNC layer at the glass side (details can be found in Figure S22). A higher CRI for ideal white-light illumination can be expected if the red and yellowish-green PeNCs are replaced by other broad-spectrum emitters like organic fluorescent powder.

Furthermore, besides its use in PeLEDs, this strategy could also be extended to other types of white LEDs, such as inorganic, quantum dot, and hybrid LEDs, etc., to improve their light extraction in chips, which broadly contributes to the field of energy-saving lighting devices.

EXPERIMENTAL PROCEDURES

Resource Availability

Lead Contact

Further information and requests for resources and materials should be directed to and will be fulfilled by the lead contact, Hin-Lap Yip (msangusyip@scut.edu.cn).

Materials Availability

This study did not generate new unique materials.

Data and Code Availability

The data presented in this work are available from the corresponding authors upon reasonable request.

Materials and Chemicals

Nickel(II) acetate tetrahydrate ($Ni(CH_3COO)_2 \cdot 4H_2O$, 99.995%), ethanolamine ($NH_2CH_2CH_2OH$, 99.5%), ethanol (99.8%), poly(9-vinylcarbazole) (PVK, average M_n ranging from 25,000 to 50,000 g mol^{-1}), CsBr (99.999%), $PbBr_2$ (99.999%), chlorobenzene (CB, anhydrous, 99.8%) and ethyl acetate (EA, anhydrous, 99.8%) were purchased from Sigma-Aldrich. Phenylethylammonium bromide (PEABr, 99.5%), *iso*-propylammonium bromide (IPABr, 99.5%), phenylbutylammonium bromide (PBABr, 99.5%) and formamidinium bromide (FABr) were purchased from Xi'an Polymer Light Technology Corp. Dimethyl sulfoxide (DMSO, >99.0%) was purchased from Acros. LiF was purchased from Alfa Aesar. 1,3,5-tris(1-phenyl-1H-benzimidazol-2-yl)benzene (TPBi) was purchased from Lumtec. Red PeNC solution ($CsPbBrI_2$ dissolved in cyclohexane, 35 mg mL^{-1}) and yellowish green PeNC solution ($CsPbBr_2I$ dissolved in cyclohexane, 10 mg ml^{-1}) were purchased from Nanjing MKNANO Tech. Co., Ltd. All chemicals were used as received.

Blue Perovskite Precursor Solution Preparation

The perovskite precursor solution (PL peak at 493 nm) was prepared using a slightly modified (formula, solution concentration, and anti-solvent) form of a previously reported method.[26] Thus, CsBr (19.2 mg), $PbBr_2$ (55.1 mg), PEABr (24.2 mg), and IPABr (8.4 mg), in a fixed molar ratio of 3:5:4:2, were dissolved in DMSO (1 mL) under continuous stirring for 12 h at room temperature, with the molar concentration of Pb^{2+} fixed at 0.15 M. For the pure blue perovskite precursor solution (PL peak at 476 nm), CsBr, FABr, $PbBr_2$, and PBABr with molar ratio fixed at 7:3:10:14 were dissolved in DMSO under continuous stirring for 12 h at room temperature, keeping the molar concentration of Pb^{2+} at 0.1 M, yielding the composition of $PBABr_{1.4}(Cs_{0.7}FA_{0.3}PbBr_3)$.[9]

PeLED Fabrication

Patterned ITO-coated glass substrates (15 mm × 15 mm) were cleaned by sonication in detergent, deionized water, acetone, and isopropyl alcohol and then

dried at 65°C in a baking oven. After a 5-min oxygen plasma treatment of ITO substrates, NiO_x layers were deposited onto the ITO substrates using a previously reported method.[27] To prepare the NiO_x precursor solution, a 1:1 molar ratio of $Ni(CH_3COO)_2{\cdot}4H_2O$ and $NH_2CH_2CH_2OH$ were dissolved in ethanol under continuous stirring for 12 h at 70°C, keeping the concentration of Ni^{2+} at 0.1 M. All NiO_x films were deposited by spin-casting the 0.45 μm-PTFE filtered NiO_x precursor solution at 3,000 rpm for 50 s and then baking them at 270°C for 45 min in ambient air. After cooling to room temperature, the NiO_x-coated substrates were subject to a 5-min oxygen plasma treatment.[28] Then, layers of PVK (dissolved in CB, 8 mg ml^{-1}) were spin-coated (2,000 rpm for 30 s) onto the substrates, and the resulting coated substrates were annealed at 150°C for 30 min in an N_2-filled glovebox. Then, the blue perovskite precursor solution was spin-coated onto the NiO_x/PVK films at 4,000 rpm for 2 min, with EA (100 μL) was introduced as an anti-solvent at 26 s after the beginning of spin-coating. Subsequently, the resulting films were annealed at 70°C for 10 min. Finally, TPBi (32 nm) and LiF/Al/Ag/LiF electrodes (1/1/9/10 nm) were deposited using a thermal evaporation system under a high vacuum of $<1 \times 10^{-6}$ Torr. The device's active area was 8 mm^2, as defined by the overlapping area of the ITO and Al/Ag electrodes. For the two-color WPeLEDs, the red PeNC solution was spin-coated on top of the LiF/Al/Ag/LiF electrode at the spin speed of 450 (Point A), 350 (Point B), and 300 rpm (Point C) for 2 min. For the three-color WPeLEDs, red PeNC solution was spin-coated on top of the LiF/Al/Ag/LiF electrode at 450 rpm for 2 min while yellowish green PeNC solution was spin-coated on the glass side at 400 rpm for 2 min.

Perovskite Film and Device Characterizations

Ultraviolet-visible absorption spectra were recorded on an HP 8453E spectrophotometer (Agilent Technologies Co. Ltd., America). Steady-state PL was recorded using a Horiba Fluorolog system (HORIBA Ltd., Japan) equipped with a single grating, using a monochromatized Xe lamp as the excitation source. PLQYs of the perovskite films were recorded on a commercial PLQY measurement system (Ocean Optics) with excitation from a 365-nm LED. Atmospheric ultraviolet photoelectron spectra were recorded on an AC-3 system with a standard deviation of ±0.02 eV (Riken Keiki Co., Ltd). The crystalline structure of the perovskite films was investigated using an X-ray diffractometer (PANalytical X'pert PRO, Netherlands) equipped with a Cu-Kα X-ray tube, using ITO/NiO_x/PVK/perovskite sample. The scanning electron microscope (SEM) images of the sample structure of ITO/NiO_x/PVK/perovskite were obtained with a Hitachi Regulus 8100 SEM (Japan). The atomic force microscope measurements were carried out using a Digital Instrumental Multimode Nanoscope IIIa in tapping mode. The cross-sectional STEM images, high-resolution transmission electron microscope image, and energy dispersive spectroscopy measurement were taken with a FIB-TEM Helios Nanolab 450S. The optical parameters of *n* (refractive index) and *k* (extinction coefficient) for different films were measured using a dual rotating-compensator Mueller matrix ellipsometer (ME-L ellipsometer, Wuhan Eoptics Technology, China). The current density–voltage and luminance–voltage curves, EL spectrum, EQE and operating lifetime of the PeLED were recorded simultaneously on a commercial system (XPQY-EQE-350-1100, Guangzhou Xi Pu Optoelectronics Technology Co., Ltd., China) that was equipped with an integrating sphere (GPS-4P-SL, Labsphere) and a photodetector array (S7031-1006, Hamamatsu Photonics). All of the device characterization tests of the PeLEDs were carried out in an N_2-filled glovebox.

FDTD Simulation

The simulation was carried out with the Lumerical 2019b FDTD software package and was based on the device structure shown in Figure 1B and the *n*/*k* values shown in Figure S3. A three-dimensional simulation was used with periodic boundary conditions for x and y planes, and boundary conditions of perfectly matched layer for the z planes. A dipole light source was placed in a sky-blue perovskite emitter and three individual simulations with different dipole orientations were conducted, to mimic light generated in an isotropic emitter. Frequency-domain field and power monitors were added in different functional layers within the device to record the transmitted light power and far-field light power. The ratio of photons trapped in and absorbed by the layer was calculated as the ratio between the light-power in the layer and the light-source power, which was measured by a three-dimensional box monitor surrounding the dipole light source.

SUPPLEMENTAL INFORMATION

Supplemental Information can be found online at https://doi.org/10.1016/j.joule.2020.12.008.

ACKNOWLEDGMENTS

This study was financially supported by the Guangdong Major Project of Basic and Applied Basic Research (no. 2019B030302007), the National Natural Science Foundation of China (nos. 91733302, 51903086, and 62075065), and the China Postdoctoral Science Foundation (nos. 2019M650197 and 2020T130204). Moreover, we highly appreciate the help from Dr. Artem A. Bakulin at Imperial College London for useful discussions on the manuscript. We also thank Mr. Jiajie Zeng for assisting in the angle-dependent luminance measurement.

AUTHOR CONTRIBUTIONS

Ziming Chen conceived the idea and designed the experiments. Z.L. and Ziming Chen fabricated the blue and white PeLEDs and carried out the device characterizations. Z.L., Ziming Chen, Zhen Chen, R.X., G.Z., and L.C. carried out the perovskite film characterizations. S.-J.S. and J.P. provided the atmospheric ultraviolet photoelectron spectra measurement and useful discussion on the results. Ziming Chen carried out the FDTD simulation. Ziming Chen and Z.L. provided equal contributions to this study. All authors contributed to the manuscript. Ziming Chen, Z.L., and H.-L.Y. analysed the data and wrote the manuscript. Ziming Chen and H.-L.Y. led the project. H.-L.Y. and Y.C. supervised the research.

DECLARATION OF INTERESTS

The authors declare no competing interests.

Received: September 1, 2020
Revised: November 12, 2020
Accepted: December 9, 2020
Published: January 4, 2021

REFERENCES

1. Yuan, M., Quan, L.N., Comin, R., Walters, G., Sabatini, R., Voznyy, O., Hoogland, S., Zhao, Y., Beauregard, E.M., Kanjanaboos, P., et al. (2016). Perovskite energy funnels for efficient light-emitting diodes. Nat. Nanotechnol. *11*, 872–877.

2. Lin, K., Xing, J., Quan, L.N., de Arquer, F.P.G., Gong, X., Lu, J., Xie, L., Zhao, W., Zhang, D., Yan, C., et al. (2018). Perovskite light-emitting diodes with external quantum efficiency exceeding 20 per cent. Nature *562*, 245–248.

3. Chiba, T., Hayashi, Y., Ebe, H., Hoshi, K., Sato, J., Sato, S., Pu, Y., Ohisa, S., and Kido, J. (2018). Anion-exchange red perovskite quantum dots with ammonium iodine salts for highly efficient light-emitting devices. Nat. Photon. *12*, 681–687.

4. Cao, Y., Wang, N., Tian, H., Guo, J., Wei, Y., Chen, H., Miao, Y., Zou, W., Pan, K., He, Y., et al. (2018). Perovskite light-emitting diodes based on spontaneously formed submicrometre-scale structures. Nature *562*, 249–253.

5. Xu, W., Hu, Q., Bai, S., Bao, C., Miao, Y., Yuan, Z., Borzda, T., Barker, A.J., Tyukalova, E., Hu, Z., et al. (2019). Rational molecular passivation for high-performance perovskite light-emitting diodes. Nat. Photonics *13*, 418–424.

6. Zhao, B., Bai, S., Kim, V., Lamboll, R., Shivanna, R., Auras, F., Richter, J.M., Yang, L., Dai, L., Alsari, M., et al. (2018). High-efficiency perovskite–polymer bulk heterostructure light-emitting diodes. Nat. Photon. *12*, 783–789.

7. Fang, Z., Chen, W., Shi, Y., Zhao, J., Chu, S., Zhang, J., and Xiao, Z. (2020). Dual passivation of perovskite defects for light-emitting diodes with external quantum efficiency exceeding 20%. Adv. Funct. Mater. *30*, 1909754.

8. Li, Z., Chen, Z., Yang, Y., Xue, Q., Yip, H.L., and Cao, Y. (2019). Modulation of recombination zone position for quasi-two-dimensional blue perovskite light-emitting diodes with efficiency exceeding 5%. Nat. Commun. *10*, 1027.

9. Liu, Y., Cui, J., Du, K., Tian, H., He, Z., Zhou, Q., Yang, Z., Deng, Y., Chen, D., Zuo, X., et al. (2019). Efficient blue light-emitting diodes based on quantum-confined bromide perovskite nanostructures. Nat. Photonics *13*, 760–764.

10. Wang, Q., Wang, X., Yang, Z., Zhou, N., Deng, Y., Zhao, J., Xiao, X., Rudd, P., Moran, A., Yan, Y., and Huang, J. (2019). Efficient sky-blue perovskite light-emitting diodes via photoluminescence enhancement. Nat. Commun. *10*, 5633.

11. Cho, H., Jeong, S.H., Park, M.H., Kim, Y.H., Wolf, C., Lee, C.L., Heo, J.H., Sadhanala, A., Myoung, N., Yoo, S., et al. (2015). Overcoming the electroluminescence efficiency limitations of perovskite light-emitting diodes. Science *350*, 1222–1225.

12. Xiao, Z., Kerner, R.A., Zhao, L., Tran, N.L., Lee, K.M., Koh, T.-W., Scholes, G.D., and Rand, B.P. (2017). Efficient perovskite light-emitting diodes featuring nanometre-sized crystallites. Nat. Photon. *11*, 108–115.

13. Dong, Y., Wang, Y.K., Yuan, F., Johnston, A., Liu, Y., Ma, D., Choi, M.J., Chen, B., Chekini, M., Baek, S.-W., et al. (2020). Bipolar-shell resurfacing for blue LEDs based on strongly confined perovskite quantum dots. Nat. Nanotechnol. *15*, 668–674.

14. Zhao, L., Lee, K.M., Roh, K., Khan, S.U.Z., and Rand, B.P. (2019). Improved outcoupling efficiency and stability of perovskite light-emitting diodes using thin emitting layers. Adv. Mater. *31*, e1805836.

15. Shi, X.-B., Liu, Y., Yuan, Z., Liu, X., -Miao, K., Wang, Y., Lenk, J., Reineke, S.,S., and Gao, F. (2018). Optical energy losses in organic-inorganic hybrid perovskite light-emitting diodes. Adv. Opt. Mater. *6*, 1800667.

16. Mao, J., Lin, H., Ye, F., Qin, M., Burkhartsmeyer, J.M., Zhang, H., Lu, X., Wong, K.S., and Choy, W.C.H. (2018). All-perovskite emission architecture for white light-emitting diodes. ACS Nano *12*, 10486–10492.

17. Sun, R., Lu, P., Zhou, D., Xu, W., Ding, N., Shao, H., Zhang, Y., Li, D., Wang, N., Zhuang, X., et al. (2020). Samarium-doped metal halide perovskite nanocrystals for single-component electroluminescent white light-emitting diodes. ACS Energy Lett. *5*, 2131–2139.

18. Shen, Y., Cheng, L.P., Li, Y.Q., Li, W., Chen, J.D., Lee, S.T., and Tang, J.X. (2019). High-efficiency perovskite light-emitting diodes with synergetic outcoupling enhancement. Adv. Mater. *31*, e1901517.

19. Zhang, Q., Tavakoli, M.M., Gu, L., Zhang, D., Tang, L., Gao, Y., Guo, J., Lin, Y., Leung, S.F., Poddar, S., et al. (2019). Efficient metal halide perovskite light-emitting diodes with significantly improved light extraction on nanophotonic substrates. Nat. Commun. *10*, 727.

20. Zhang, Q., Zhang, D., Gu, L., Tsui, K.H., Poddar, S., Fu, Y., Shu, L., and Fan, Z. (2020). Three-dimensional perovskite nanophotonic wire array-based light-emitting diodes with significantly improved efficiency and stability. ACS Nano *14*, 1577–1585.

21. Heckmann, J., Pufahl, K., Franz, P., Grosse, N.B., Li, X., and Woggon, U. (2018). Plasmon-enhanced nonlinear yield in the Otto and Kretschmann configurations. Phys. Rev. B *98*, 115415.

22. Barnes, W.L., Dereux, A., and Ebbesen, T.W. (2003). Surface plasmon subwavelength optics. Nature *424*, 824–830.

23. Xu, H., Wang, X., Li, Y., Cai, L., Tan, Y., Zhang, G., Wang, Y., Li, R., Liang, D., Song, T., and Sun, B. (2020). Prominent heat dissipation in perovskite light-emitting diodes with reduced efficiency droop for silicon-based display. J. Phys. Chem. Lett. *11*, 3689–3698.

24. Court, I.N., and von Willisen, F.K. (1964). Frustrated total internal reflection and application of its principle to laser cavity design. Appl. Opt. *3*, 719–726.

25. Cho, C., Zhao, B., Tainter, G.D., Lee, J.Y., Friend, R.H., Di, D., Deschler, F., and Greenham, N.C. (2020). The role of photon recycling in perovskite light-emitting diodes. Nat Commum *11*, 611.

26. Xing, J., Zhao, Y., Askerka, M., Quan, L.N., Gong, X., Zhao, W., Zhao, J., Tan, H., Long, G., Gao, L., et al. (2018). Color-stable highly luminescent sky-blue perovskite light-emitting diodes. Nat. Commun. *9*, 3541.

27. Manders, J.R., Tsang, S.-W., Hartel, M.J., Lai, T.-H., Chen, S., Amb, C.M., Reynolds, J.R., and So, F. (2013). Solution-processed nickel oxide hole transport layers in high efficiency polymer photovoltaic cells. Adv. Funct. Mater. *23*, 2993–3001.

28. Wang, T., Ding, D., Zheng, H., Wang, X., Wang, J., Liu, H., and Shen, W. (2019). Efficient inverted planar perovskite solar cells using ultraviolet/ozone-treated NiO_x as the hole transport layer. Sol. RRL *3*, 1900045.